Brodogradnja Volume 76 Number 2 (2026) 77206

University of Zagreb
Faculty of Mechanical
Engineering and Naval
Architecture

journal homepage: www.brodogradnja.fsb.hr

Brodogradnja

An International Journal of Naval Architecture and
Ocean Engineering for Research and Development

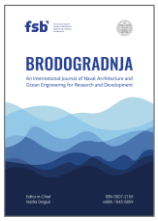

Robust trajectory tracking of surface vessels in ice floe sea state via discrete integral sliding-mode control and Gaussian process regression

Qiaosheng Zhao[1,2], *Chao Peng*[2], *Chaoxu Mu*[1], *Shaocheng Li*[3,*], *Dejun Li*[2]

[1] *Tianjin University, No.92 Weijin Road, Nankai District, 300072, Tianjin, China*
[2] *China Ship Scientific Research Center, No.222 Shanshui East Road, Binhu District, 214142, Wuxi, Jiangsu, China*
[3] *Harbin Engineering University, No.1777 Sansha Road, Westcoast New District, 266000, Qingdao, Shandong, China*

ARTICLE INFO

Keywords:
Unmanned surface vessels
Gaussian process regression
Discrete integral sliding-mode control
Stochastic discrete-time systems

ABSTRACT

By considering the disturbance caused by ice floes in polar regions, the trajectory tracking control problem for uncertain unmanned surface vessels (USVs) is investigated in this paper. USVs for trajectory tracking missions in polar regions are required to not only overcome common disturbances and perturbations such as model uncertainties and environmental disturbances caused by winds, waves and currents, but it must also consider the stochastic resistance generated by ice floes. However, studies on the stochastic model of ice floes resistance on USVs are insufficient, making it difficult to a design tracking controller. This paper proposes a discrete integral sliding-mode control (DISMC) with a disturbance observer based on Gaussian process regression (GPR) technique, which could steer uncertain USVs to track predefined trajectories under disturbance without knowing its upper bound. Compared to the existing methods for USV control, (1) to the best of our knowledge, this study is among the first to address the trajectory tracking control problem of USVs in ice-floe sea conditions; (2) a novel fully data-driven disturbance observer is proposed that approximates the mean and autocorrelation function of the lumped uncertainties without requiring prior knowledge about the stochastic ice resistance; and (3) a novel DISMC given the autocorrelation function of uncertainties instead of the uncertain upper bound is proposed and proved to be stable with a probability of 1. The proposed method offers a significant approach for controlling USVs in ice-covered sea areas.

1. Introduction

The environment in polar regions has garnered global attention. Unmanned and autonomous exploration through predefined trajectories in ice-covered ocean areas is a vital technology for future scientific research and commercial exploitation in polar regions [1]. During explorations and expeditions through extreme environments in polar regions, the motion of unmanned surface vessels (USVs) is affected by winds, waves, currents, and the uncertain resistance caused by ice floes. A reliable trajectory tracking strategy under perturbations and disturbances is a key technology that determines the success or failure of the exploitation missions. From the perspective of stochastic analysis theory, the spectrum of ocean waves, winds, and currents has been well established and verified since the 1990s [2]. The maneuverability of ships under the influence

* Corresponding author.
E-mail address: lishaocheng@hrbeu.edu.cn

https://doi.org/10.21278/brod77206
Received 3 September 2025; Received in revised form 14 October 2025; Accepted 18 October 2025
Available online 5 November 2025
ISSN 0007-215X; eISSN 1845-5859

of winds, waves, and currents has been extensively investigated [3]. However, prior knowledge about the stochastic properties of disturbance forces caused by ice floes is insufficient [4-6]. Thus, the control strategies that could steer USVs in ice-covered ocean areas are required to not only overcome common disturbances and perturbations such as model uncertainties and environmental disturbances caused by winds, waves, and currents, but it must also consider the stochastic resistance generated by ice floes. However, traditional trajectory tracking control methods often require the stochastic properties of the uncertainties, such as the upper bound, to be known beforehand, making it a significant challenge when addressing the tracking problem in the aforementioned scenario — this places a premium on trajectory tracking control for uncertain USVs.

Trajectory tracking control methods for USVs can be classified in two aspects: model-free controls and model-based controls. PID or PD control are conventional model-free methods, which have limited robustness to uncertainties and disturbances [7,8]. To improve their adaptability, adaptive variants have been developed, for example an adaptive proportional–integral–derivative controller based on soft actor–critic (SAC-PID) has been proposed in [9], demonstrating enhanced robustness in uncertain marine environments. Intelligent algorithm such as fuzzy logic and artificial neural network (ANN) is then developed to improve the adaptability and robustness of PID or PD control to uncertainties [10,11]. However, these methods still provide insufficient precision when addressing uncertain systems. In addition, approaches based on fuzzy logic may provide high steady-state error. Data-driven theories, like deep learning (DL), reinforcement learning (RL) and etc, are advanced model-free methods for USVs control, which enables USVs to learn control strategies from datasets. However, large-scale real-world dataset are needed for the learning-based methods, and the stability of the closed-loop system must be carefully validated. To further improve the control performance, model-based control methods, such as the sliding mode control (SMC) [12], backstepping control [13-15] and model predictive control [16-19] are developed. Nonlinear adaptive heading control for underactuated surface vessels with constrained input and sideslip angle compensation has been investigated in [20], providing improved maneuverability under realistic dynamic constraints. Moreover, in practical navigation scenarios, trajectory and speed control in curved channels has also been studied [21], which further highlights the importance of developing robust control strategies under constrained waterways. Model-based methods require either the accurate dynamic model of the USV or the stochastic properties of uncertainties, which are also sensitive to uncertainties. Disturbances observer methods are developed to improve the adaptiveness and robustness of the tracking control by approximating model perturbations and disturbances [22]. The disturbances observer is designed to estimate uncertainties and disturbances in the system online and feedback the estimation into the controller to compensate for uncertainties and disturbances. Machine learning (ML) methods, which provide the ability to approximate nonlinear functions, can also be applied to build such observer, making it possible to learn unknown dynamics online, while imposing a significant computational burden. Model-based methods provide improved precision and dynamic performance, however, they often lack robustness and adaptability. Conversely, model-free methods yield strong control qualities but require extensive real-world datasets and significant computational resources. Developing hybrid approaches that leverage the strengths of both model-based and model-free techniques is significant to enhancing the robustness and adaptability of USVs in uncertain environments, but it has been considered challenging - it is this aspect that is addressed here.

Controllers based on SMC theory are considered a promising way to develop hybrid methods. As a robust control method, SMC has been widely used for unmanned systems. By utilizing SMC, the system states can be maintained on the sliding surface, ensuring robustness of the closed-loop system against uncertainties and disturbances. However, the reaching phase decreases the effectiveness of SMC such that the stability of the closed-loop system should be carefully verified. To overcome this issue, the integral SMC (ISMC) is proposed that could eliminate the reaching phase while providing a nominal system (the system without unknown dynamics) that defines the dynamics of the matched disturbance system [23]. The switching term in SMC effectively suppresses the disturbance, although it may cause the chattering phenomenon. A possible approach is to introduce DOs to estimate the lumped uncertainties, which could reduce the switching gain thereby enhancing adaptability while mitigating chattering effects [24,25]. Furthermore, using ML methods to establish DOs suggests a hybrid approach. This method combines the precision and good dynamic

performance of model-based approaches with the benefits of model-free methods in approximating uncertainties.

Although conventional hybrid methods have shown promising results in control performance and eliminating chattering, these methods rely on expert experience or large prior experimental data [26]. Hybrid methods integrating an ML-based DO into a controller with an SMC structure show effective performance; however, several issues remain. First, the estimation error of the learning-based DO is often assumed to be bounded [26]. For ANN-based DOs, this assumption can be guaranteed according to the Weierstrass approximation theorem [27]. ANN-DOs have been successfully applied in marine control, such as adaptive SMC for USVs under wave disturbances [25], but they require substantial training data and offer limited interpretability due to their black-box nature. In contrast, probabilistic methods like the invariant extended Kalman filter [28] and Gaussian process regression (GPR) [29] provide posterior distributions (often zero-mean Gaussian) that do not always satisfy bounded error assumptions, invalidating traditional stability criteria reliant on deterministic bounds.

To address these, GPR has emerged as a powerful tool in control literature for non-parametric disturbance estimation, particularly in stochastic and data-scarce environments. GPR-based DOs enable online approximation of nonlinear disturbances without assuming prior distributions, leveraging kernel functions to model correlations in residuals [30]. Recent works have demonstrated GPR-DOs in rejecting unmodeled dynamics for inverted pendulums and urban air mobility systems, where GPR compensates for multi-dimensional disturbances using small datasets (e.g., <500 samples), outperforming ANN in sample efficiency by 2-3 times. In marine applications, GPR has been integrated with model predictive control for trajectory tracking under uncertain currents and fixed-time control for USVs, quantifying uncertainty via confidence intervals to enhance robustness. Compared to ANN-DOs, GPR-DOs provide not only point estimates but also variance predictions, facilitating probabilistic stability analysis in discrete-time systems. Accordingly, the controller design and stability analysis given the posterior estimation of uncertainties are worthy of further investigations. Moreover, ML methods are developed based on discrete-time dynamic models, but proofs of closed-loop stability for existing hybrid methods are often in continuous form [25,31]. Considering the advantages of easy implementation and small-sample estimation of probabilistic DOs, it is necessary to investigate the design of a hybrid controller and criteria for closed-loop stability for a discrete SMC system with posterior estimation following a given probability distribution [32,33].

Trajectory tracking control for USVs in uncertain environments such as ice-covered ocean areas shows both theoretical and practical challenges. Theoretically, the spectrum of stochastic resistance caused by ice floes is not fully established, making it impossible to regulate control parameters as specifically as when addressing wind wave disturbances. Although feasible controllers may be established using an arbitrarily upper bound on the lumped uncertainties, it may lead to problems such as excessive gain or chattering. In practice, it is a significant challenge to obtain real-world data on the stochastic disturbance caused by ice floes, both from numerical simulations and from real-world environments, that are sufficiently large and accurate to train effective controllers. Consequently, novel control strategies need to be developed.

Considering the disturbance caused by ice floes in polar regions, the trajectory tracking control problem for uncertain unmanned surface vessels (USVs) is investigated in this paper. A discrete integral sliding-mode control (DISMC) with a fully data-driven DO, based on Gaussian process regression (GPR) technique, is proposed, which could steer uncertain USVs to track predefined trajectories under disturbance without knowing its upper bound. Theoretically, the control parameters can be adaptively implemented based on the observed lumped uncertainties. In practice, GPR-based observer does not require large, real-world datasets, while the stability of the closed-loop system can be ensured. By implementing the proposed method, an uncertain USV can trace given trajectories in ice-covered ocean areas, which— to the best of our knowledge— has not been explicitly addressed in existing studies. Numerical simulations illustrate the superior performance of the proposed controller in comparison to the existing methods. The main contributions of this paper can be summarized as follows:

1. A novel hybrid method that consists of a DISMC and a GPR-based DO is proposed for solving the trajectory tracking control problem for USVs under disturbance caused by ice floes.

2. Compared to the existing disturbance observer [22,25,26,34], a novel disturbance observer based on GPR technique is proposed that the mean function and autocorrelation function of the lumped uncertainties can be estimated in a fully data-driven manner without requiring prior knowledge.
3. Compared to the conventional ISMC [25,26,35], a novel DISMC given the autocorrelation function of uncertainties instead of the uncertain upper bound is proposed and proved to be stable with a probability of 1.

This paper is organized as follows. Section 2 introduces the necessary preliminaries including the discrete 3 degrees of freedom dynamic equations of surface vessels, assumptions considered in this paper, and problem descriptions. For a discrete stochastic system with bounded uncertainties, a trajectory tracking control based on discrete integral sliding mode control is proposed and the closed-loop system is proved to be stable in Section 3. A disturbance observer based on Gaussian process regression is proposed in Section 4, which improves the control quality under stochastic uncertainties. A discrete integral sliding mode control considering Gaussian white noise and the proof of stability are also given in Section 4. The nominal control that stabilizes the dynamic system without uncertainties based on the backstepping technique is given in Section 5. Numerical simulations are conducted and discussed in Section 6, which demonstrate the superior performance in comparison with traditional trajectory tracking methods for surface vessels. Section 7 concludes this paper.

Notation. Throughout this paper, $\mathbb{R}^{n\times m}$ denotes the $n\times m$ dimensional Euclidean space. $\mathbb{N}_0$ denotes the set of all natural numbers. $|v|$ and $\|v\|$ denotes the 1-norm, i.e., the sum of the absolute values of the elements, and the 2-norm of vector v, respectively. $\Pr(X)$ and $\mathbb{E}[X]$ denote the probability and the mathematical expectations of a stochastic variable X, respectively. $I_n \in \mathbb{R}^{n\times n}$ represents a $n\times n$ identity matrix. For a vector $Y=[y_1 \quad y_2 \quad \dots \quad y_n]$, $\operatorname{sgn}(Y)=[\operatorname{sign}(y_1) \quad \operatorname{sign}(y_2) \quad \dots \quad \operatorname{sign}(y_n)]:\mathbb{R}^n\to\mathbb{R}^n$ represents the vector sign function, where $\operatorname{sign}(y):\mathbb{R}\to\mathbb{R}$ is given by:

$$\operatorname{sign}(y)=\begin{cases}1, y>0\\ 0, y=0\\ -1, y<0\end{cases} \tag{1}$$

The superscript $\top$ is used to denote the transpose of a vector or matrix.

2. Preliminaries and problem formulation

2.1 Discrete 3 degrees of freedom dynamics of a surface vessel

The 3 degrees of freedom (3-DOF, surge, sway, and yaw) dynamic model of a USV considered in this paper is given as follows. As shown in Figure 1, the surge, sway, and yaw motion are represented as x, y and ψ, and surge, sway, and yaw velocities are represented as v_x, v_y and v_ψ, respectively.

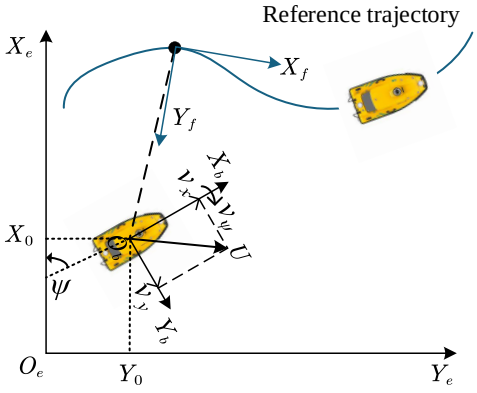

Fig. 1 Definition of reference coordinate frames of the vessel dynamics

Let $\eta = \begin{bmatrix} x & y & \psi \end{bmatrix}^\top \in \mathbb{R}^3$ and $v = \begin{bmatrix} v_x & v_y & v_\psi \end{bmatrix}^\top \in \mathbb{R}^3$, the 3-DOF dynamic equations of the surface vessel are given by [36]:

$$\begin{cases} \dot{\eta} = J(\eta)v \\ M\dot{v} + C(v)v + D(v)v + G(\eta) = \tau + F_{ice}(\eta, v, t) + F(\eta, v, t) \end{cases} \tag{2}$$

where the rotation matrix $J(\eta)$ is defined as:

$$J(\eta) = \begin{bmatrix} \cos\psi & -\sin\psi & 0 \\ \sin\psi & \cos\psi & 0 \\ 0 & 0 & 1 \end{bmatrix} \tag{3}$$

$M \in \mathbb{R}^{3\times3}$ is a symmetric positive-definite inertia matrix. $C(v) \in \mathbb{R}^{3\times3}$ represents the centripetal and Coriolis torques matrix. $D(v) \in \mathbb{R}^{3\times3}$ is the damping matrix. $G(v) \in \mathbb{R}^3$ represents the gravitational matrix. $F(\eta, v, t) \in \mathbb{R}^3$ denotes the lumped model uncertainties, including modeling uncertainties and forces and torques generated by winds, wave, and current, given by:

$$F(\eta, v, t) = \tau_{dis} - \tau_{CD} \tag{4}$$

where τ_{dis} are forces and torques generated by wind, wave, current, and τ_{CD} represents model uncertainties in $C(v)$ and $D(v)$, the details are as follows:

$$\begin{aligned} C(v) &= (1 + \delta_C) C_0(v) \\ D(v) &= (1 + \delta_D) D_0(v) \end{aligned} \tag{5}$$

where $C_0(v)$ and $D_0(v)$ correspond to the nominal parts of the dynamic model, and δ_C and δ_D account for the unmodeled or uncertain components. $F_{ice}(\eta, v, t) \in \mathbb{R}^3$ represents the additional resistance exerted by ice floes on the USV.

Let $x = \begin{bmatrix} x_1 & x_2 \end{bmatrix}^\top = \begin{bmatrix} \eta^\top & \dot{\eta}^\top \end{bmatrix}^\top$, and $u = \tau = \begin{bmatrix} \tau_x & \tau_y & \tau_\psi \end{bmatrix}^\top$, we have:

$$\begin{aligned} \dot{x}_2 &= \dot{J}(\eta)v + J(\eta)M^{-1}\tau + J(\eta)M^{-1}(-C(v)v - D(v)v - G(\eta) - F(\eta, v, t) - F_{ice}(\eta, v, t)) \\ &= \mathcal{G}(\eta)\tau + \mathcal{G}(\eta)(-C(v)v - D(v)v - G(\eta) - F_{ice}(\eta, v, t)) + \dot{J}(\eta)v - \mathcal{G}(\eta)(F(\eta, v, t)) \\ &= \mathcal{G}(\eta)u + \mathcal{F}(\eta, v) + \mathcal{D}(\eta, v, t) \end{aligned} \tag{6}$$

where:

$$\begin{aligned} &\mathcal{G}(\eta) = J(\eta)M^{-1}, \\ &\mathcal{F}(\eta, v) = \mathcal{G}(\eta)(-C(v)v - D(v)v - G(\eta) - F_{ice}(\eta, v, t)) + \dot{J}(\eta)v \\ &\mathcal{D}(\eta, v, t) = \mathcal{G}(\eta)(F(\eta, v, t)). \end{aligned} \tag{7}$$

The 3-DOF dynamic model can be described as an affine nonlinear system given by:

$$\begin{cases} \dot{x}_1 = x_2 \\ \dot{x}_2 = \mathcal{G}u + \mathcal{F}(\eta, v) + \mathcal{D}(\eta, v, t) \end{cases} \tag{8}$$

Assume a sampling interval of $T \in [0, \mathcal{T}] \subset \mathbb{R}_+$, where $\mathcal{T}$ denoting the upper bound on time, $k \in [0, \frac{\mathcal{T}}{T}] \subset \mathbb{N}_0$, and $x(k) = \left[x_1(k), x_2(k)\right]^\top$, and denoting:

$$\begin{aligned} \mathcal{G}(k) &= \mathcal{G}(\eta(k)) \\ \mathcal{F}(k) &= \mathcal{F}(\eta(k), v(k)) \\ \mathcal{D}(k) &= \mathcal{D}(\eta(k), v(k), k) \end{aligned} \tag{9}$$

the discrete 3-DOF dynamics of the surface vessel is given by:

$$\begin{cases} x_1(k+1) = Tx_2(k) + x_1(k) \\ x_2(k+1) = T(\mathcal{F}(k) + \mathcal{G}(k)u(k) + \mathcal{D}(k)) + x_2(k) \end{cases} \tag{10}$$

Note that $\mathcal{G}(k)$ is invertible and $\mathcal{D}(k)$ is a stochastic process representing the lumped uncertainties. The nominal system is given by:

$$\begin{cases} x_1(k+1) = Tx_2(k) + x_1(k) \\ x_2(k+1) = T(\mathcal{F}(k) + \mathcal{G}(k)u(k)) + x_2(k) \end{cases} \tag{11}$$

System (10) is a stochastic nonlinear system. The reason for that a discrete-time dynamic model is considered is given as follows. If the continuous-time model is utilized, the system with lumped uncertainty becomes a stochastic differential system. In this case, the calculus of lumped uncertainty process must be considered and the synthesis method for deterministic systems cannot be applied. In contrast, using the description in Problem 2, system (11) becomes a Markov process and the sequence of states $\{x_k\}$ becomes a Markov chain. Thus, the discrete stochastic systems theory is capable of system synthesis.

2.2 Problem formulation

In this paper, following assumptions according to system (10) would be applied.

Assumption 1. *The reference position trajectory $\{x_d(k)\}$ of system (10) is Lipschitz continuous, i.e., its sufficiently high order derivatives are known and bounded.*

Assumption 2([13]). *All states in system (10) are available for feedback and bounded.*

Assumption 3. *The lumped uncertainty $\mathcal{D}(k)$ in system (10) is a zero-mean stationary stochastic process with an autocorrelation function of $R(k_1, k_2)$.*

Remark 1. *Based on Assumption 1 and Assumption2, reference trajectories would be smooth enough to satisfy the maneuverability of USVs in practice and the states feedback control is feasible (neglecting the measurement errors). Assumption 3 is a commonly used assumption when addressing the stochastic system.*

Traditional trajectory tracking control problem generally assume that the lumped uncertainty $\mathcal{D}(k)$ is bounded, i.e., for every k, there exists a constant γ such that:

$$\| \mathcal{D}(k) \| \leq \gamma(k) \tag{12}$$

Under this assumption, the traditional trajectory tracking control problem is given as follows.

Problem 1. *Considering system (10) with Assumption 1, Assumption 2, and Eq.(12), design a control sequence $\{u(k)\}$ making the tracking errors $e(t) = x_1(k) - x_d(k)$, where $x_d(k)$ satisfies Assumption 1 denotes the reference trajectory, converges to 0.*

However, when solving the trajectory tracking problem involving disturbance caused by ice floes, the upper bound of the lumped uncertainty cannot be appropriately defined. An arbitrary γ may increase control

gain and amplify chattering. Besides, if data-driven approaches are employed to estimate the uncertainties, only ANN-based DOs can provide estimations with guaranteed error bounds. The challenge lies in the substantial amount of prior data required to train such network estimators – data is often difficult to obtain in real-world applications (for instance, the mechanical properties of sea ice floes in a specific region). To relax the assumption of bounded uncertainties and enable USVs to achieve trajectory control without prior knowledge about disturbance, Assumption 3 is introduced. This assumption is also capable of methods estimating the autocorrelation function of a stochastic process, particularly when leveraging a Bayesian framework. Therefore, the problem to be solved in this paper is given as follows.

Problem 2. *Considering system (10) with Assumption 1, Assumption 2, and Assumption 3, design a control sequence* $\{u(k)\}$ *making the tracking errors* $e(t)$ *converges to 0.*

Problem 1 is solved using the DISMC method in Section 3, which is also the foundation for solving Problem 2.

3. Design of DISMC for trajectory tracking control for surface vessels under bounded stochastic uncertainties

The change of tracking errors over time is defined as:

$$\begin{aligned}\Delta e(k) &= e(k+1) - e(k) \\ &= x_1(k+1) - x_1(k) - (x_d(k+1) - x_d(k)) \\ &= Tx_2(k) - \Delta x_d(k)\end{aligned} \tag{13}$$

The filter error is defined as:

$$s(k) = \frac{1}{T}\Delta e(k) + \lambda e(k) = x_2(k) - \frac{1}{T}\Delta x_d(k) + \lambda e(k) \tag{14}$$

where λ is a constant. Differentiating Eq. (14) with respect to k and applying Eq. (10), there is:

$$\begin{aligned}\Delta s(k) &= s(k+1) - s(k) \\ &= x_2(k+1) - x_2(k) - \frac{1}{T}\left(\Delta x_d(k+1) - \Delta x_d(k)\right) + \lambda(e(k+1) - e(k)) \\ &= \mathcal{F}(k) + \mathcal{G}(k)u(k) + \mathcal{D}(k) - \frac{1}{T}(\Delta x_d(k+1) - \Delta x_d(k)) + \lambda\Delta e(k).\end{aligned} \tag{15}$$

Let $u(k) = u_s(k) + u_0(k)$, where $u_0(k)$ represents the nominal control which is utilized to control the nominal dynamics, i.e., the system without uncertainties, given by:

$$\Omega = \mathcal{F}(k) + \mathcal{G}(k)u_0(k) - \frac{1}{T}(\Delta x_d(k+1) - x_d(k)) + \lambda\Delta e(k) \tag{16}$$

and $u_s(k)$ is the robust term. The sliding surface is defined as:

$$\sigma(k) = s(k) - s(0) - \sum_{i=0}^{k-1}\left[\mathcal{F}(i) + \mathcal{G}(i)u_0(i) + \mu(i) - \frac{1}{T}(\Delta x_d(i+1) - x_d(i)) + \lambda\Delta e(i)\right] \tag{17}$$

Thus, the differentiation of the sliding mode surface with respect to k can be calculated as:

$$\begin{aligned}\Delta\sigma(k) &= \sigma(k+1)-\sigma(k)\\ &= \Delta s(k)-\mathcal{F}(k)+\mathcal{G}(k)u_0(k)-\frac{1}{T}(\Delta x_d(k+1)-x_d(k))+\lambda\Delta e(k)\\ &= \mathcal{G}(k)u_s(k)+\mathcal{D}(k)\end{aligned} \tag{18}$$

The design of the nominal control $u_0(k)$ are addressed in Section 5. The following theorem gives a solution to $u_s(k)$ that stabilizes system (15).

Theorem 1. *Consider discrete-time system (18) with Assumption 1, 2 and 3. For*

$$\begin{aligned}&\forall\ b\in\left\{\left(1-\sqrt{2},0\right)\cup\left(2,1+\sqrt{2}\right)\right\}\\ &\cap\left\{\left[-\infty,1-\sqrt{n}\frac{\gamma}{|\sigma(k)|}\right]\right.\\ &\left.\cup\left[1+\sqrt{n}\frac{\gamma}{|\sigma(k)|},\infty\right]\right\}\end{aligned} \tag{19}$$

and $\forall a\in[a_1,a_2]$, *where*

$$\begin{cases}a_1=\dfrac{(1-b)|\sigma(k)|-\sqrt{(1-b)^2|\sigma(k)|^2-n\gamma^2}}{n}\\ a_2=\dfrac{(1-b)|\sigma(k)|+\sqrt{(1-b)^2|\sigma(k)|^2-n\gamma^2}}{n}\end{cases} \tag{20}$$

with n *denoting the dimension of the system, if*

$$u_s(k)=\mathcal{G}^{-1}(k)(-a\ sgn(\sigma(k))-b\sigma(k)) \tag{21}$$

then $\sigma(k)=0$ *is globally a.s. exponentially stable, i.e., for* $\forall\sigma(0)\in\mathbb{R}^3,\Pr\left[\lim_{k\to\infty}\|\ \sigma(k)\|=0\right]=1$.

Proof . Substituting Eq. (21) with Eq. (18), we have:

$$\sigma(k+1)=-a\ sgn(\sigma(k))+(1-b)\sigma(k)+\mathcal{D}(k) \tag{22}$$

Define a Lyapunov function candidate given by:

$$V_1(k)=\sigma(k)^\top\sigma(k) \tag{23}$$

such that:

$$\begin{aligned}&\mathbb{E}\left[V_1(x(k+1))\middle|\ x(k)\right]\\ &=\mathbb{E}\left[(m_1(k)+\mathcal{D}(k))^\top(m_1(k)+\mathcal{D}(k))\right]\\ &=\mathbb{E}\left[m_1(k)^\top m_1(k)\right]+2\mathbb{E}\left[\mathcal{D}(k)^\top m_1(k)\right]+\mathbb{E}\left[\mathcal{D}(k)^\top\mathcal{D}(k)\right]\\ &=m_1(k)^\top m_1(k)+R(0)\\ &=a^2n+(1-b)^2\sigma(k)^\top\sigma(k)-2a(1-b)|\sigma(k)|+R(0)\end{aligned} \tag{24}$$

where $m_1(k)=-a\ sgn(\sigma(k))+(1-b)\sigma(k)$ such that:

$$\begin{aligned}&\mathbb{E}\left[V_1(x(k+1))\middle|\ x(k)\right]-V_1(x(k))\\&\le a^2n+\left[(1-b)^2-1\right]\sigma(k)^\top\sigma(k)-2a(1-b)|\sigma(k)|+\gamma^2\end{aligned}\tag{25}$$

If the following inequality holds:

$$\begin{cases}0<(1-b)^2-1<1\\a^2n-2a(1-b)|\sigma(k)|+\gamma^2\le 0\end{cases}\tag{26}$$

then:

$$\mathbb{E}\left[V_1(x(k+1))\middle|\ x(k)\right]-V_1(x(k))\le\alpha V_1(x(k))\tag{27}$$

Moreover, making $c_1=c_2=1$, we have:

$$c_1\left\|x(k)\right\|^2\le V_1(x(k))\le c_2\left\|x(k)\right\|^2\tag{28}$$

Eq. (27) and Eq. (28) imply that the Expectation of the derivative of the Lyapunov function $V_1(x(k))$ is not larger than a radial unbounded, positive definite function that has an infinitesimal upper bound. According to [37], we have:

$$\Pr\left[\lim_{k\to\infty}\|\ \sigma(k)\|=0\right]=1\tag{29}$$

Eq. (29) implies that the probability of that the system trajectory converges to the equilibrium point $\sigma(k)=0$ is 1.

We now solve a and b. The first inequality of Eq. (26) suggests that:

$$b\in\left(1-\sqrt{2},0\right)\cup\left(2,1+\sqrt{2}\right)\tag{30}$$

To ensure that the second inequality in Eq. (26) holds, b must also satisfy:

$$4(1-b)^2|\sigma(k)|^2-4n\gamma^2\ge 0\tag{31}$$

implying that:

$$b\in\left[-\infty,1-\sqrt{n}\frac{\gamma}{|\sigma(k)|}\right]\cup\left[1+\sqrt{n}\frac{\gamma}{|\sigma(k)|},\infty\right]\tag{32}$$

Based on Eq. (30) and Eq. (32), we proof Eq. (19). Moreover, if Eq. (32) holds, the quadratic inequality with respect to a must have solutions in $\mathbb{R}$, i.e., $a_1\le a\le a_2$, where a_1 and a_2 are given by Eq. (20). Therefore, the stability of the sliding surface is guaranteed.

4. Design of DISMC for tracking control with Gaussian process regression of surface vessels

In this section, an observer based on GPR technique is developed that can estimate the lumping uncertainties $\mathcal{D}(k)$. By employing the proposed observer, a novel DISMC is proposed.

4.1 Disturbance observer based on Gaussian process regression

The following gives the design of GPR-based observer. GPR provides a method for predicting the output of a stochastic process in function space using supervised learning approaches, which has significant

advantages in nonlinear regression and few-shot learning. To inference $\mathcal{D}(k)$ using $\{x(k)\}$, a Gaussian process regressor is designed.

The training data set is defined as $\{X(k), \mathbb{D}(k)\}$ where:

$$\begin{cases} X(k) = \{x(0), x(1), \ldots, x(k)\} \\ \mathbb{D}(k) = \{\mathcal{D}(0), \mathcal{D}(1), \ldots, \mathcal{D}(k)\} \end{cases} \tag{33}$$

Considering Assumption 2, $\mathcal{D}(k)$ can be calculated as:

$$\mathcal{D}(i) = \frac{x_2(k+1) - x_2(k+1|\ k)}{T} \tag{34}$$

at time $k+1$ with $x_2(k+1|k)$ denoting the predicted state at $k+1$ employing the nominal system (11). Assuming that $\mathbb{D}(k-1)$, $\mathcal{D}(k)$, and the joint distribution of $\mathbb{D}(k-1)$ and $\mathcal{D}(k)$ are Gaussian distributions given by:

$$\begin{aligned} &\mathbb{D}(k-1) \sim \mathcal{N}\left(\boldsymbol{\mu}_{k-1}, \boldsymbol{\Lambda}_{k-1,k-1}\right) \\ &\mathcal{D}(k) \sim \mathcal{N}\left(\boldsymbol{\mu}_{k}, \boldsymbol{\Lambda}_{k,k}\right) \\ &\begin{bmatrix} \mathbb{D}(k-1) \\ \mathcal{D}(k) \end{bmatrix} \sim \mathcal{N}\left(\boldsymbol{\mu}, \boldsymbol{\Sigma}\right) \end{aligned} \tag{35}$$

where $\boldsymbol{\mu} = \begin{bmatrix} \boldsymbol{\mu}_{k-1} & \boldsymbol{\mu}_{k} \end{bmatrix}^{\top}$ and the covariance matrix $\boldsymbol{\Sigma}$ is defined as:

$$\begin{aligned} \boldsymbol{\Sigma} &= \begin{bmatrix} \boldsymbol{\Sigma}_{k-1,k-1} & \boldsymbol{\Sigma}_{k-1,k} \\ \boldsymbol{\Sigma}_{k,k-1} & \boldsymbol{\Sigma}_{k,k} \end{bmatrix} \\ &= \begin{bmatrix} K(X(k-1), X(k-1)) & K\left(X(k-1), x(k)\right) \\ K\left(x(k), X(k-1)\right) & K\left(x(k), x(k)\right) \end{bmatrix} \end{aligned} \tag{36}$$

where $K(\cdot,\cdot)$ is the covariance matrix function that defines the covariance of data sets $\{x(k)\}$, which can be calculated using predefined kernel function $k(\cdot,\cdot)$ as:

$$K = \begin{bmatrix} k\left(x(0), x(0)\right) & k\left(x(0), x(1)\right) & \cdots & k\left(x(0), x(k)\right) \\ k\left(x(1), x(0)\right) & k\left(x(1), x(1)\right) & \cdots & k\left(x(1), x(k)\right) \\ \vdots & \vdots & \ddots & \vdots \\ k\left(x(k), x(0)\right) & k\left(x(k), x(1)\right) & \cdots & k\left(x(k), x(k)\right) \end{bmatrix} \tag{37}$$

Using the GPR method, the disturbance $\mathcal{D}(k)$ can be estimated using the state trajectory $\mathbb{D}(k-1)$ as shown in Lemma 1.

Lemma 1. *If $\mathbb{D}(k-1)$, $\mathcal{D}(k)$, and the joint distribution of them are Gaussian distributions defined as Eq. (35), the conditional distribution of $\mathcal{D}(k)$ given $\mathbb{D}(k-1)$ is also Gaussian, i.e.:*

$$\Pr\left[\tilde{\mathcal{D}}(k) \middle| \mathbb{D}(k-1)\right] \sim \mathcal{N}\left(\mu(k), \Gamma(k)\right), \tag{38}$$

where

$$\begin{cases} \mu(k) = K\left(x(k), X(k-1)\right) K(X(k-1), X(k-1))^{-1} \mathbb{D}(k-1) \\ \Gamma(k) = K\left(x(k), x(k)\right) - K\left(x(k), X(k-1)\right) \mathcal{K} \\ \mathcal{K} = K(X(k-1), X(k-1))^{-1} K(X(k-1), x(k)) \end{cases} \tag{39}$$

Proof. The precision matrix of the joint distribution can be calculated as:

$$\mathbf{\Lambda} = \begin{bmatrix} \mathbf{\Lambda}_{k-1,k-1} & \mathbf{\Lambda}_{k-1,k} \\ \mathbf{\Lambda}_{k,k-1} & \mathbf{\Lambda}_{k,k} \end{bmatrix} = \mathbf{\Sigma}^{-1} \tag{40}$$

The quadratic form in the exponent of the Gaussian distribution given by Eq. (35) can be calculated as:

$$\begin{aligned} & -\frac{1}{2}(\mathbb{D}(k) - \boldsymbol{\mu})^{\top} \mathbf{\Sigma}^{-1} (\mathbb{D}(k) - \boldsymbol{\mu}) \\ & = -\frac{1}{2}\left(\mathcal{D}(k) - \boldsymbol{\mu}_k\right)^{\top} \mathbf{\Lambda}_{k,k} \left(\mathcal{D}(k) - \boldsymbol{\mu}_k\right) \\ & -\frac{1}{2}\left(\mathcal{D}(k) - \boldsymbol{\mu}_k\right)^{\top} \mathbf{\Lambda}_{k,k-1} \left(\mathbb{D}(k-1) - \boldsymbol{\mu}_{k-1}\right) \\ & -\frac{1}{2}\left(\mathbb{D}(k-1) - \boldsymbol{\mu}_{k-1}\right)^{\top} \mathbf{\Lambda}_{k-1,k} \left(\mathcal{D}(k) - \boldsymbol{\mu}_k\right) \\ & -\frac{1}{2}\left(\mathbb{D}(k-1) - \boldsymbol{\mu}_{k-1}\right)^{\top} \mathbf{\Lambda}_{k,k} \left(\mathbb{D}(k-1) - \boldsymbol{\mu}_{k-1}\right) \end{aligned} \tag{41}$$

As a function of $\mathcal{D}(k)$, Eq. (41) is again a quadratic form, and hence the corresponding conditional distribution $\Pr\left[\mathcal{D}(k) \middle| \mathbb{D}(k-1)\right]$ is still Gaussian. Denoting the means and covariance of the conditional distribution as $\mu(k)$ and $\Gamma(k)$, respectively, we have:

$$\Pr\left[\tilde{\mathcal{D}}(k) \middle| \mathbb{D}(k-1)\right] \sim \mathcal{N}\left(\mu(k), \Gamma(k)\right) \tag{42}$$

We now derive the expressions for $\mu(k)$ and $\Gamma(k)$. Consider the quadratic form in Eq. (41) as a function of $\mathcal{D}(k)$, coefficients entering the second order term in $\mathcal{D}(k)$ of Eq. (41) can be calculated as:

$$-\frac{1}{2}(\mathcal{D}(k) - \boldsymbol{\mu}_k)^{\top} \mathbf{\Lambda}_{k,k} (\mathcal{D}(k) - \boldsymbol{\mu}_k) \tag{43}$$

Therefore, the covariance of the conditional distribution is given by:

$$\Gamma(k) = \mathbf{\Lambda}_{k,k}^{-1} \tag{44}$$

Now consider all the terms in Eq. (41) that are linear in $\mathcal{D}(k)$ given by:

$$\mathcal{D}(k)^{\top} \left\{ \mathbf{\Lambda}_{k,k} \boldsymbol{\mu}_k - \mathbf{\Lambda}_{k,k-1} \left(\mathbb{D}(k-1) - \boldsymbol{\mu}_{k-1}\right) \right\} \tag{45}$$

Thus, we have:

$$\begin{aligned} \mu(k) &= \mathbf{\Lambda}_{k,k}^{-1} \left\{ \mathbf{\Lambda}_{k,k} \boldsymbol{\mu}_k - \mathbf{\Lambda}_{k,k-1} \left(\mathbb{D}(k-1) - \boldsymbol{\mu}_{k-1}\right) \right\} \\ &= \boldsymbol{\mu}_k + \mathbf{\Lambda}_{k,k}^{-1} \mathbf{\Lambda}_{k,k-1} \left(\mathbb{D}(k-1) - \boldsymbol{\mu}_{k-1}\right) \end{aligned} \tag{46}$$

According to the matrix inversion lemma, we have:

$$\begin{aligned}\boldsymbol{\Lambda}_{k,k}^{-1} &= \boldsymbol{\Lambda}_{k-1,k-1}^{-1} + \boldsymbol{\Lambda}_{k,k-1}\left(\boldsymbol{\Lambda}_{k,k}\right)^{-1}\boldsymbol{\Lambda}_{k,k-1}^{\top} \\ &= K(X(k),X(k))^{-1} - K(X(k),x(k))\mathcal{K}\end{aligned} \tag{47}$$

where

$$\mathcal{K} = K(X(k-1),X(k-1))^{-1}K(X(k-1),x(k)) \tag{48}$$

is the Schur complement of $\boldsymbol{\Sigma}$. This ends the proof.

Based on Lemma 1, the maximum a posteriori estimation of $\mathcal{D}(k)$ is $\mu(k)$. According to the law of large numbers, the estimation errors decrease proportionally with an increase in the number of sample points, implying that:

$$\lim_{k\to\infty}\left\|\Gamma(k)\right\| = 0 \tag{49}$$

Besides, the covariance function $k(x,x')$ applied in this paper is the radial basis function (RBF) kernel given by:

$$k(x,x') = \sigma_f^2 \exp\left[\frac{-\left(x-x'\right)^2}{2l^2}\right] \tag{50}$$

where σ_f^2 is the variance of the output and l is the length scale parameter.

Eq. (42) also suggests that the estimation error is a zero-means white Gaussian noise (ZWGN) with a covariance $\Gamma(k)$. Finally, the observer can be expressed as:

$$\mathcal{D}(k) = \mu(k) + W(k), W(k) \sim \mathcal{N}(0,\Gamma(k)) \tag{51}$$

For real-time USV control, the GPR-based disturbance observer adopts a sliding-window scheme to prevent unbounded dataset growth. At each control step k, the most recent 100 samples are retained ($N \le 100$) and older samples are discarded. The model is re-trained every 20 control steps (at step 10 for initialization) because the floating-ice disturbance varies slowly relative to the controller sampling interval of $T = 10ms$. Overall, the online implementation integrates a sliding-window data management scheme and scheduled model updates to maintain stable performance under stochastic disturbances while keeping the computation tractable, which is summarized in Algorithm 1.

Algorithm 1 Online GPR-Based Disturbance Observer (GPR-DO)

Parameter Initialization: Sliding window size N_w =100; retraining interval $N_{update} = 20$; controller sampling period $T = 100ms$.

GP Model Initialization:

1: Initialize empty dataset $\mathcal{D} = \varnothing$ and GP hyperparameters.

2: Train the initial GP model (mean $\mu_0(\cdot)$, covariance $\Gamma_0(\cdot)$) using a few nominal samples or prior knowledge.

Online Update (executed at each control step k):

1: Collect the current system state $x_k = [x, y, \psi, u, v, r]^T$ and compute the residual disturbance sample $(x_k, \hat{d}_k)$ from model–measurement differences.

2: Append the new sample $(x_k, \hat{d}_k)$ to the dataset $\mathcal{D}$.

3: **If** $|\mathcal{D}| > N_w$ **then**

delete the oldest sample to maintain a fixed-size window.

end if

4: **If** mod $(k, N_{update}) = 0$ or $k \le 10$ **then**

Retrain the GP model using the samples in $\mathcal{D}$.

Update the mean and covariance functions $\mu_k(\cdot)$ and $\Gamma_k(\cdot)$ by maximizing the marginal likelihood.

end if

5: Predict the disturbance for the next step:

$\hat{d}_{k+1} = \mu_k(x_{k+1})$, $\sum_{k+1} = \Gamma_k(x_{k+1}, x_{k+1})$

6: Output $\hat{d}_{k+1}$ to the DISMC controller for real-time disturbance compensation.

7: Proceed to the next control step $k \leftarrow k+1$

This windowed and periodic-update strategy limits the cubic training cost of conventional GPR from $O(N^3)$ to a fixed and manageable level.

Remark 2. *The observer Eq.(51) is a fully data-driven method that could estimate the lumped uncertainties in a probabilistic manner, which does not require any prior knowledge of the system model. This makes it particularly suitable for USV control problems where the ice resistance is unknown a priori.*

4.2 Design of DISMC for trajectory tracking under white Gaussian noise

The dynamic equations of surface vessels with disturbance observer based on GPR can be described as:

$$\begin{cases} x_1(k+1) = Tx_2(k) + x_1(k) \\ x_2(k+1) = T(\mathcal{F}(k) + \mathcal{G}(k)u(k) + \mu(k) + W(k)) + x_2(k) \end{cases} \tag{52}$$

Using the methodology proposed in Section 3, we derive the DISMC method for system (52). Let $e(k) = x_1(k) - x_2(k)$ denote the tracking error and $x_d(k) = \eta_d(k) = \begin{bmatrix} x(k) & y(k) & \psi(k) \end{bmatrix}^\top$ denote the reference trajectory. The differentiation of the tracking error can be calculated as:

$$\begin{aligned}\Delta e(k) &= e(k+1)-e(k)\\ &= x_1(k+1)-x_1(k)-(x_d(k+1)-x_d(k))\\ &= Tx_2(k)-\Delta x_d(k)\end{aligned} \tag{53}$$

The filter error is still represented by:

$$s(k)=\frac{1}{T}\Delta e(k)+\lambda e(k)=x_2(k)-\frac{1}{T}\Delta x_d(k)+\lambda e(k) \tag{54}$$

Differentiating Eq. (54), there is:

$$\begin{aligned}\Delta s(k) &= s(k+1)-s(k)\\ &= x_2(k+1)-x_2(k)-\frac{1}{T}(\Delta x_d(k+1)-\Delta x_d(k))+\lambda(e(k+1)-e(k))\\ &= \mathcal{F}(k)+\mathcal{G}(k)u(k)+\mu(k)+W(k)-\frac{1}{T}(\Delta x_d(k+1)-\Delta x_d(k))+\lambda\Delta e(k)\end{aligned} \tag{55}$$

The corresponding nominal system is given by:

$$\Omega=\mathcal{F}(k)+\mathcal{G}(k)u_0(k)+\mu(k)-\frac{1}{T}(\Delta x_d(k+1)-x_d(k))+\lambda\Delta e(k) \tag{56}$$

The controller is still given as $u(k)=u_s(k)+u_0(k)$ where $u_0(k)$ represents the nominal control and $u_s(k)$ represents the robust term. The sliding surface is defined as:

$$\sigma(k)=s(k)-s(0)-\sum_{i=0}^{k-1}\left[\mathcal{F}(i)+\mathcal{G}(i)u_0(i)+\mu(i)-\frac{1}{T}(\Delta x_d(i+1)-x_d(i))+\lambda\Delta e(i)\right] \tag{57}$$

The differentiation of the sliding surface can be calculated as:

$$\begin{aligned}\Delta\sigma(k) &= \sigma(k+1)-\sigma(k)\\ &= \Delta s(k)-\mathcal{F}(k)+\mathcal{G}(k)u_0(k)-\frac{1}{T}(\Delta x_d(k+1)-x_d(k))+\lambda\Delta e(k)\\ &= \mathcal{G}(k)u_s(k)+W(k)\end{aligned} \tag{58}$$

The design of the nominal control is addressed in Section 5. We now give Theorem 2 that solve the robust term.

Theorem 2. *Consider discrete-time system (18) with Assumption 1,2. For any given* $a,b\in\mathbb{R}$ *satisfying*

$$\begin{aligned}&a\in[a_1,a_2]\\ &b\in\left\{\left(1-\sqrt{2},0\right)\cup\left(2,1+\sqrt{2}\right)\right\}\cap\left\{\left[-\infty,1-\frac{\sqrt{n\Gamma(k)}}{|\sigma(k)|}\right]\cup\left[1+\frac{\sqrt{n\Gamma(k)}}{|\sigma(k)|},\infty\right]\right\}\end{aligned} \tag{59}$$

where

$$\begin{aligned}a_1&=\frac{(1-b)|\sigma(k)|-\sqrt{(1-b)^2|\sigma(k)|^2-n\Gamma(k)}}{n}\\ a_2&=\frac{(1-b)|\sigma(k)|+\sqrt{(1-b)^2|\sigma(k)|^2-n\Gamma(k)}}{n}\end{aligned} \tag{60}$$

with n *denoting the dimension of the system, there exists a control sequence*

$$u_s(k) = \mathcal{G}^{-1}(k)(-a\,\mathrm{sgn}(\sigma(k)) - b\sigma(k)) \tag{61}$$

such that the closed-loop system of system (55) globally a.s. exponentially stable, i.e., $\Pr[\lim_{k\to\infty} \| \sigma(k) \| = 0] = 1$

Proof. The closed-loop system can be derived by substituting Eq. (61) with Eq. (58) as:

$$\sigma(k+1) = -a\,\mathrm{sgn}(\sigma(k)) + (1-b)\sigma(k) + W(k) \tag{62}$$

Denoting $m_2(k) = -a\,\mathrm{sgn}(\sigma(k)) + (1-b)\sigma(k)$, the Lyapunov function candidate is defined as:

$$V_2(k) = \sigma(k)^\top \sigma(k) \tag{63}$$

Considering $\mathbb{E}[W(k)] = 0$, we have:

$$\begin{aligned} &\mathbb{E}\left[V_2(x(k+1)) \middle| \ x(k)\right] \\ &= \mathbb{E}\left[(m_2(k) + W(k))^\top (m_2(k) + W(k))\right] \\ &= \mathbb{E}\left[m_2(k)^\top m_2(k)\right] + 2\mathbb{E}\left[W(k)^\top m_2(k)\right] n + \mathbb{E}\left[W(k)^\top W(k)\right] \\ &= m_2(k)^\top m_2(k) + \Gamma(k) = a^2 n + (1-b)^2 \sigma(k)^\top \sigma(k) - 2a(1-b)\,|\,\sigma(k)\,| + \Gamma(k) \end{aligned} \tag{64}$$

Thus, the differentiation of the Lyapunov function can be calculated as:

$$\begin{aligned} &\mathbb{E}\left[V_2(x(k+1)) \middle| \ x(k)\right] - V_2(x(k)) \\ &= a^2 n + (1-b)^2 \sigma(k)^\top \sigma(k) - 2a(1-b)\,|\,\sigma(k)\,| - \sigma(k)^\top \sigma(k) + \Gamma(k) \\ &= a^2 n + \left[(1-b)^2 - 1\right] \sigma(k)^\top \sigma(k) - 2a(1-b)\,|\,\sigma(k)\,| + \Gamma(k) \end{aligned} \tag{65}$$

If a and b satisfy:

$$\begin{cases} a^2 n - 2a(1-b)\,|\,\sigma(k)\,| + \Gamma(k) \le 0 \\ 0 < (1-b)^2 - 1 < 1 \end{cases} \tag{66}$$

then:

$$\mathbb{E}\left[V_2(x(k+1)) \middle| \ x(k)\right] - V_2(x(k)) \le \alpha V_2(x(k)) \tag{67}$$

Moreover, let $c_1 = c_2 = 1$, we have:

$$c_1 \left\| x(k) \right\|^2 \le V_2(x(k)) \le c_2 \left\| x(k) \right\|^2 \tag{68}$$

Eq. (67) and Eq. (68) imply that the Expectation of the derivative of the Lyapunov function $V_1(x(k))$ is not larger than a radial unbounded, positive definite function that has an infinitesimal upper bound. According to [33], we have:

$$\Pr\left[\lim_{k\to\infty} \| \sigma(k) \| = 0\right] = 1 \tag{69}$$

Eq. (69) implies that the probability that the system trajectory converges to the equilibrium point $\sigma(k) = 0$ is 1.

Eq. (66) suggests that:

$$\begin{cases} 0<(1-b)^2-1<1 \\ 4(1-b)^2\,|\,\sigma(k)\,|^2-4n\Gamma(k)\geq 0 \end{cases} \tag{70}$$

Thus, we have:

$$b\in\left\{\left(1-\sqrt{2},0\right)\cup\left(2,1+\sqrt{2}\right)\right\}\cap\left\{\left[-\infty,1-\frac{\sqrt{n\Gamma(k)}}{|\,\sigma(k)\,|}\right]\cup\left[1+\frac{\sqrt{n\Gamma(k)}}{|\,\sigma(k)\,|},\infty\right]\right\} \tag{71}$$

Meanwhile, a must satisfy:

$$\begin{cases} a_1\leq a\leq a_2 \\ a_1=\dfrac{(1-b)\,|\,\sigma(k)\,|-\sqrt{(1-b)^2\,|\,\sigma(k)\,|^2-n\Gamma(k)}}{n} \\ a_2=\dfrac{(1-b)\,|\,\sigma(k)\,|+\sqrt{(1-b)^2\,|\,\sigma(k)\,|^2-n\Gamma(k)}}{n} \end{cases} \tag{72}$$

Eq. (71) and (72) guarantees that Eq. (66) holds and further guarantees the stability of system (62).

Under the control law Eq. (61), the system trajectory will converge to the sliding surface with probability 1, even in the presence of uncertainties. In the next section, we will implement the backstepping control to design the nominal controller $u_0(k)$ to ensure that the system trajectory converges to the desired trajectory.

5. Design of the nominal controller implementing backstepping control

The nominal system considered in the section is given by:

$$\begin{cases} x_1(k+1)=Tx_2(k)+x_1(k) \\ x_2(k+1)=T(\mathcal{F}(k)+\mathcal{G}(k)u_0(k)+\mu(k))+x_2(k) \end{cases} \tag{73}$$

Firstly, denoting $z_1(k)=x_1(k)-x_d(k)$, we have:

$$z_1(k+1)=Tx_2(k)-\Delta x_d(k)+z_1(k) \tag{74}$$

If $Tx_2(k)-\Delta x_d(k)=-k_1z_1(k)$ and $0<k_1<2$, then Eq. (74) is stable. The virtual control errors is defined as:

$$\alpha_1(z_1(k))=-k_1z_1(k)+\Delta x_d(k) \tag{75}$$

Secondly, denoting $z_2(k)=Tx_2(k)-\alpha_1(z_1(k))$, we have:

$$\begin{aligned} &z_2(k+1)-z_2(k) \\ &=T(\mathcal{F}(k)+\mathcal{G}(k)u_0(k)+\mu(k))-(-k_1(z_1(k+1)-z_1(k))+\Delta x_d(k+1)-\Delta x_d(k)) \\ &=T(\mathcal{F}(k)+\mathcal{G}(k)u_0(k)+\mu(k))-k_1^2z_1(k)-(\Delta x_d(k+1)-\Delta x_d(k)) \end{aligned} \tag{76}$$

If

$$T(\mathcal{F}(k)+\mathcal{G}(k)u_0(k)+\mu(k))-(\Delta x_d(k+1)-\Delta x_d(k))=-k_2z_2(k),0<k_2<2 \tag{77}$$

then $z_2(k+1)=(1-k_2)z_2(k)-k_1^2z_1(k)$. Therefore, the closed-loop equation for system $\begin{bmatrix} z_1 & z_2 \end{bmatrix}^\top$ can be calculated as:

$$\begin{bmatrix} z_1(k+1) \\ z_2(k+1) \end{bmatrix} = \begin{bmatrix} (1-k_1)I_3 & 0 \\ -k_1^2 I_3 & (1-k_2)I_3 \end{bmatrix} \begin{bmatrix} z_1(k) \\ z_2(k) \end{bmatrix} \tag{78}$$

The characteristic equation of system (78) is given by:

$$[\lambda-(1-k_1)][\lambda-(1-k_2)]=0 \tag{79}$$

Thus, the eigenvalues of system (78) are $\lambda_1=1-k_1$ and $\lambda_2=1-k_2$. Noting that $0<k_1,k_2<2$, we have $-1<\lambda_1,\lambda_2<1$, implying that the closed-loop system (78) is globally and exponentially stable.

Finally, the nominal control is given by:

$$\begin{cases} u_0(k)=\mathcal{G}^{-1}(k)\{\frac{1}{T}[-k_2 z_2(k)+(\Delta x_d(k+1)-\Delta x_d(k))-\mu(k)-\mathcal{F}(k)]\} \\ z_2(k)=Tx_2(k)+k_1(x_1(k)-x_d(k))-\Delta x_d(k) \end{cases} \tag{80}$$

The block diagram of the overall control scheme in this paper can be seen in Figure 2.

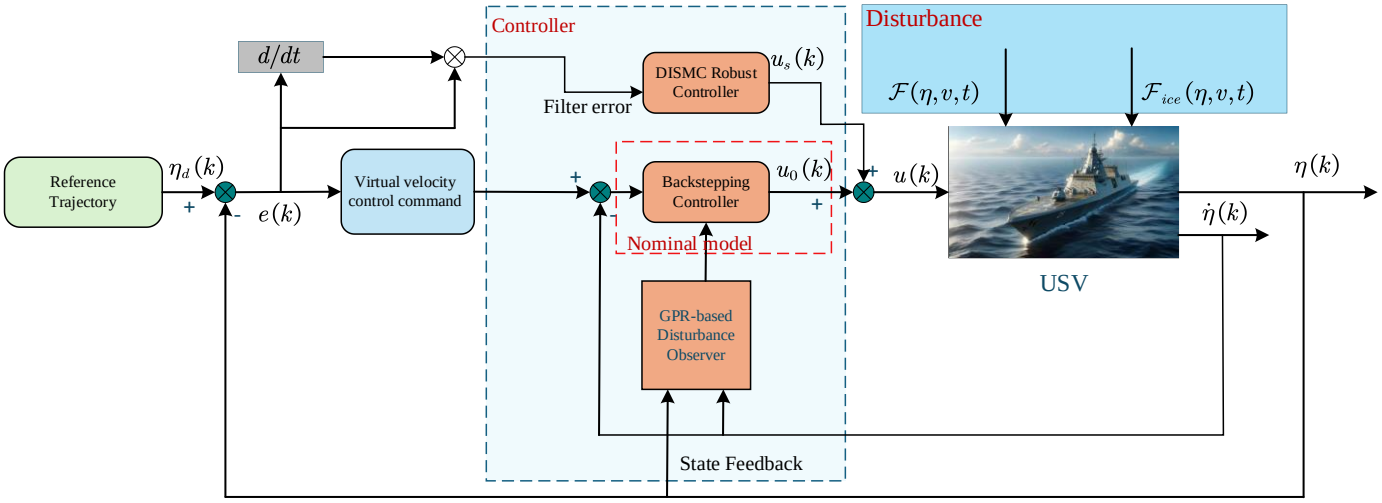

Fig. 2 The block diagram of the control scheme

6. Simulations

6.1 Simulation environment

We now give the stochastic disturbance model implemented in the simulation, including disturbance generated by ice floes, winds, waves, and currents.

According to [38,39], the resistance caused by ice floes on the USV is related to the ice thickness H, the density of ice ρ_i, Froude number F_{r_p} and the velocity of the USV V, as given by:

$$\begin{aligned} &F_{\text{ice}}(\eta,v,t)=\left[0.5C_p\rho_i BHV^2\eta^n\cdot\cos\psi \quad 0.5C_p\rho_i BHV^2\eta^n\cdot\sin\psi \quad 0\right]^{\top} \\ &C_p=k_c F_{r_p}^{-k_b} \\ &F_{r_p}=V/\sqrt{gH\eta} \end{aligned} \tag{81}$$

where C_p denotes the ice resistance coefficient depending on the modified Froude number F_{r_p}, B denotes the beam width of the vessel, k_c and k_b are empirical coefficients associated with the Froude number, and g

represents the gravitational acceleration. The modified Froude number F_{r_p} describes the dimensionless velocity of the vessel in an icy environment.

To simulate the stochastic ice disturbance, both H and ρ_i are set as colored noise given by:

$$H = H_0 + W_H(k), \rho_i = \rho_{i0} + W_\rho(k) \tag{82}$$

where both $W_H(k)$ and $W_\rho(k)$ are colored noise processes generated by low-pass filters applied to white Gaussian noises.

To further validate the statistical characteristics of the generated brash ice thickness signal, we visualize its behavior both in the time domain and the probability domain. Figure 3 shows the time-varying disturbance in brash ice thickness produced by the colored noise model, illustrating the slow-varying, inertial nature of environmental fluctuations. Figure 4 presents the probability distribution of the generated brash ice thickness, along with a fitted Gaussian curve. The histogram demonstrates that the colored noise output approximately follows a Gaussian distribution, which aligns with the assumption of zero-mean stationary stochastic processes stated in Assumption 3. This confirms the rationality of using the proposed second-order low-pass filter to simulate realistic ice thickness variations.

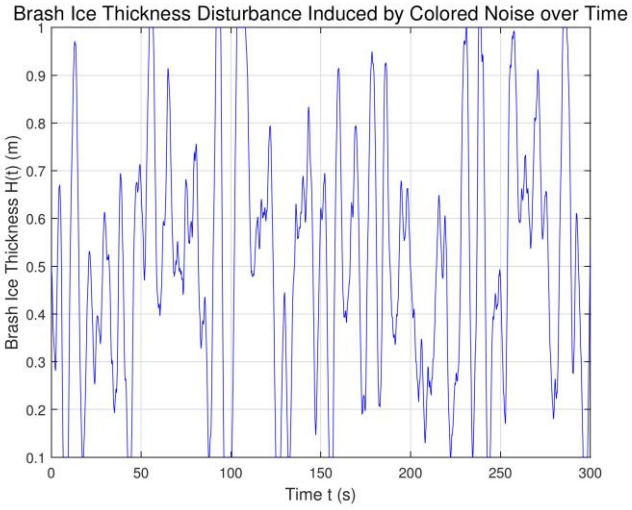

Fig. 3 Time-varying brash ice thickness disturbance modeled by colored noise

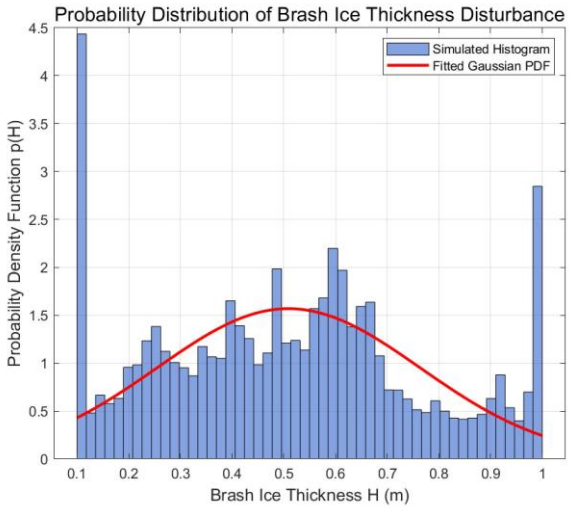

Fig. 4 Time-varying brash ice thickness disturbance modeled by colored noise

The wave spectrum model implemented in the simulation is the Pierson-Moskowitz spectrum [2] given by:

$$S(\omega) = \frac{\alpha g^2}{\omega^5} \exp\left[-\beta\left(\frac{\omega_0}{\omega}\right)^4\right] \tag{83}$$

where $\omega = 2\pi f$ with f representing the wave frequency in Hertz, $\omega_0 = g / U_{19.5}$ with $U_{19.5}$ representing the wind speed at a height of 19.5m above the sea surface, α and β are empirical coefficients. The disturbance of wind and currents are all time invariant signal. Coefficients implemented in the simulation are listed in Table 1.

To characterize the wave-induced stochastic disturbances under different wind conditions, the classical Pierson-Moskowitz spectrum is adopted, as described in Eq. (83). Figure 5 illustrates the variation of the wave energy spectral density under different wind speeds. The spectrum demonstrates a peak shifting behavior as wind speed increases, with higher wind speeds producing higher energy levels at lower frequencies. Both representations, in units of $m^2 \cdot s$ and m^2 / Hz , are shown for comparison and completeness.

Table 1. Coefficients used in the simulation environment

Parameter	Value
H_0	$0.1\,m$
ρ_{i0}	$900kg \cdot m^{-3}$
$U_{19.5}$	$5m \cdot s^{-1}$
k_c	0.6
k_b	0.9
α	8.1×10^{-3}
β	0.74

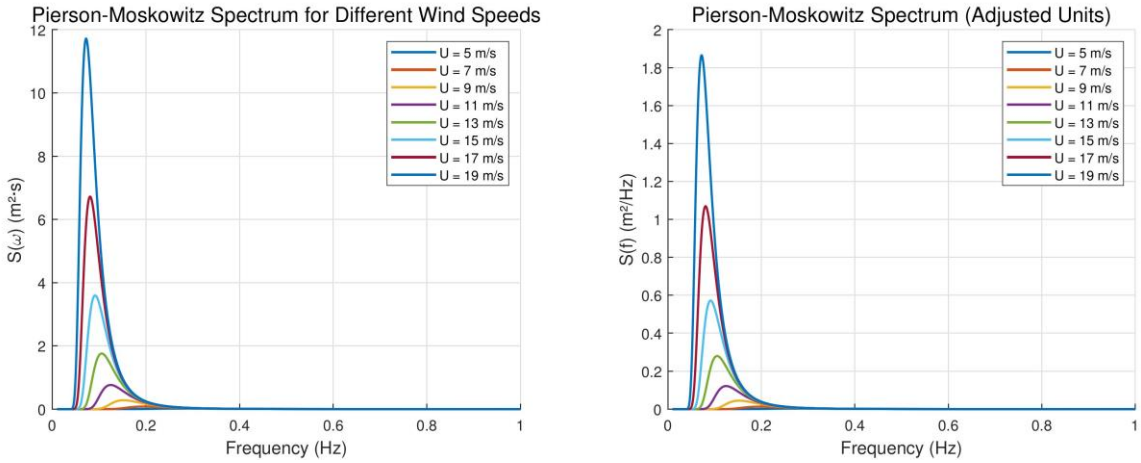

Fig. 5 Pierson-Moskowitz spectrum under varying wind speeds in units of $m^2 \cdot s$ and m^2 / Hz

6.2 Simulation results

Numerical simulations are conducted by implementing the 4th order Runge-Kutta method in the following environment. Parameters of the dynamic model of the USV implemented in the simulations are given as follows:

$$
\begin{aligned}
M &= \begin{bmatrix} m_{11} & 0 & 0 \\ 0 & m_{22} & m_{23} \\ 0 & m_{32} & m_{33} \end{bmatrix} \\
C(v) &= \begin{bmatrix} 0 & 0 & c_{13}(v) \\ 0 & 0 & c_{23}(v) \\ -c_{13}(v) & -c_{23}(v) & 0 \end{bmatrix} \\
D(v) &= \begin{bmatrix} d_{11}(v) & 0 & 0 \\ 0 & d_{22}(v) & d_{23}(v) \\ 0 & d_{32}(v) & d_{33}(v) \end{bmatrix} \\
G(\eta) &= \begin{bmatrix} 0 & 0 & 0 \end{bmatrix}^{\top}
\end{aligned}
\tag{84}
$$

where $m_{11}=25.8$, $m_{22}=24.6612$, $m_{23}=1.0948$, $m_{32}=1.0948$, $m_{33}=2.76$, $c_{13}(v)=-24.6612v-1.0948r$, $c_{23}(v)=25.8u$, and $d_{11}(v)=0.7225+1.3274|u|+5.8664u^2$, $d_{22}(v)=0.8612+36.2823|v|+8.05|r|$, $d_{23}(v)=-0.1079+0.845|v|+3.45|r|$, $d_{32}(v)=-0.1025-5.0437|v|-0.13|r|$, $d_{33}(v)=1.9-0.08|u|+0.75|r|$.

The forces and torques generated by wind, wave, and current are chosen as:

$$\tau_{dis}=\begin{bmatrix} 6u^3+6\sin(u\upsilon)+50\sin(0.5t)-50\sin(0.1t) \\ 4.5u^2+4.5\sin(\upsilon)+35\sin(0.5t-\frac{\pi}{6})-50\sin(0.3t) \\ -0.24r^3-30\sin(0.9t+\frac{\pi}{3})-30\sin(0.1t) \end{bmatrix} \tag{85}$$

We also consider the uncertainty of the model, such that:

$$\tau_{CD}=\delta_C C_0(v)v+\delta_D D_0(v)v \tag{86}$$

where $\delta_C=0.3\sin(0.52t-0.12)$ and $\delta_D=-0.25\cos(0.13t+0.67)$.

Two different cases are considered in the simulation study.

1. Case I:

   The reference trajectory can be described as:

$$\eta_d=\begin{bmatrix} x_d \\ y_d \\ \psi_d \end{bmatrix}=\begin{bmatrix} 4\sin(0.02t) \\ 2.5(1-\cos(0.02t)) \\ 0.02t \end{bmatrix} \tag{87}$$

The initial state of the vessel is set to $\eta(0)=\begin{bmatrix}1.2 & 1.2 & \frac{\pi}{3}\end{bmatrix}$ and $v(0)=[0 \quad 0 \quad 0]$.

2. Case II:

   The reference trajectory can be described as:

$$\eta_d=\begin{bmatrix} x_d \\ y_d \\ \psi_d \end{bmatrix}=\begin{bmatrix} 4\sin(0.02t) \\ 2.5\sin(2\cdot 0.02t) \\ 0.02t \end{bmatrix} \tag{88}$$

The initial state of the vessel is set to $\eta(0)=[-1 \quad 0 \quad 0]$ and $v(0)=[0 \quad 0 \quad 0]$.

The proposed method is compared with the state-of-art continuity approaches, including SMC, backstepping control, ISMC, backstepping ISMC (BISMC). In simulations using SMC, a linear sliding surface and a constant rate reaching law given by

$$\dot{s}=-Q\,sgn(s) \tag{89}$$

where $Q=[100 \quad 100 \quad 101]^\top$. The backstepping control employed in the simulations is designed using the same method mentioned in Section 5 with gains selected as $k_1=10$ and $k_2=10$. The ISMC employed in the simulations are develop based on a integrate sliding surface with parameters selected as $[5 \quad 5 \quad 5]^\top$ and a constant rate reaching law with parameters of $[100 \quad 100 \quad 101]^\top$. The BISMC employed in the simulations are develop based on [25]. The gains of the nominal controller of DISMC with GPR method employed in the

simulations are selected as $k_1 = 5$ and $k_2 = 5$. a and b of $u_s(k)$ in Eq. (19) are given as the minimum value in the solution set.

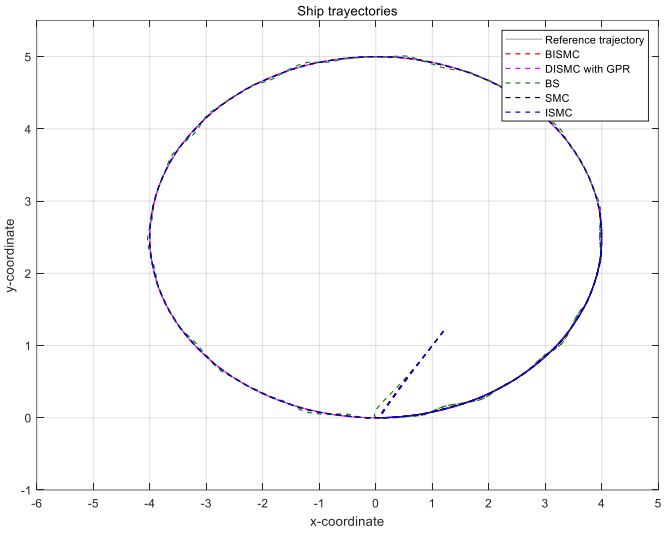

Fig. 6 Case I: Reference trajectory and real trajectory of the USV under the BS, SMC, ISMC, BISMC, and DISMC with GPR

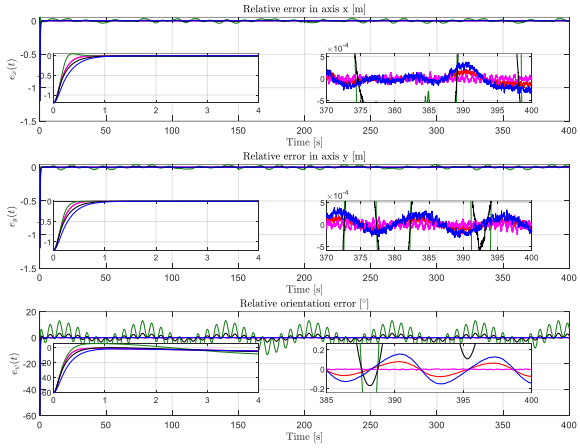

Fig. 7 Case I: Comparison in tracking error in x -axis, y -axis, and ψ -axis under the BS, SMC, ISMC, BISMC, and DISMC with GPR. Tracking errors for $t \in [0, 400]$ with a detailed view for $t \in [370, 400]$

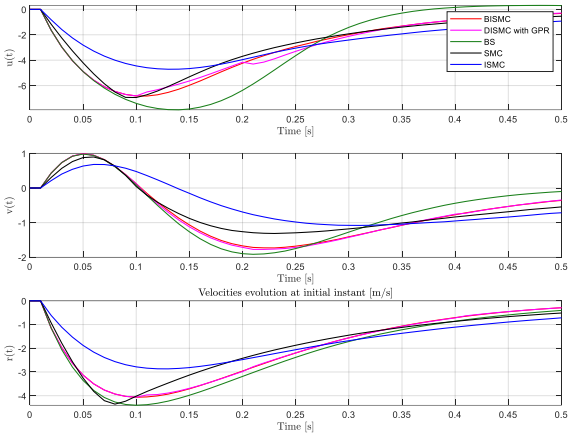

Fig. 8 Case I: Velocity trajectories of x -axis ($\dot{x}$), y -axis ($\dot{y}$), and ψ -axis ($\dot{\psi}$)under the BS, SMC, ISMC, BISMC, and DISMC with GPR. Detailed view for $t \in [0, 0.5]$ that shows the effect of the peaking phenomenon at the USV velocities

The trajectory tracking results for Case I are shown in Figure 6 - Figure 12. Figure 6 compares the reference trajectory with the trajectories generated by the five controllers. Figure 6 and Figure 7 show that the proposed method has the fastest convergence time while the convergence time of SMC method is the slowest. Moreover, the overshoot of the sliding mode controls is small compared with the backstepping control. This is because the control command provided by the backstepping control is proportional to the kinematic tracking error. Figure 8 provides a clear depiction of the initial velocity transients and the resulting peak responses, which are critical for evaluating dynamic control performance.

Comparisons of the trajectory tracking errors under the proposed method and the state-of-the-art methods are further shown in Figure 7 with mean square errors each controller listed in Table 2. Simulation results demonstrate that the mean square error of the proposed method is the smallest among all the tested methods. SMC, BC, ISMC, and BISMC methods show stronger oscillation compared to the proposed method,

which is because the proposed method employ a disturbance observer that significantly increases the robustness of the closed-loop system.

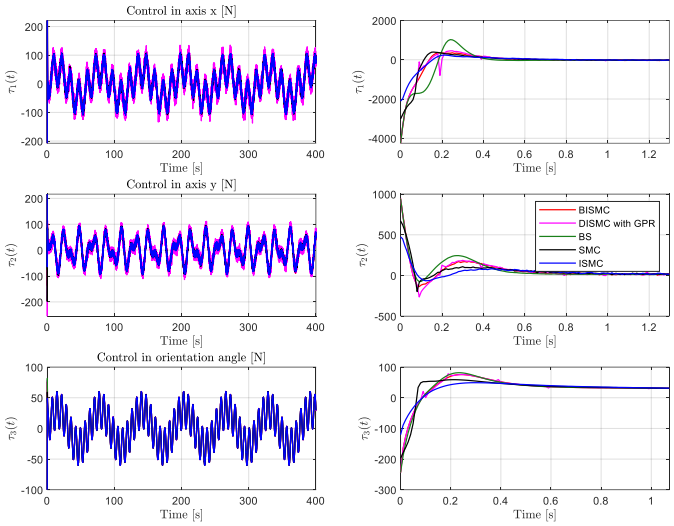

Fig. 9 Case I: Control efforts provided by BS, SMC, ISMC, BISMC, and DISMC with GPR. Control inputs for $t \in [0,400]$ in the left column. The right column shows a detailed view for $t \in [0,1.2]$ that demonstrates the peaking phenomenon at initial instants

Table 2. Comparison of mean square errors (MSEs) under the BS, SMC, ISMC, BISMC, and DISMC with GPR

Controller	**MES of $x-y$ space**	**MES of ψ space**
Backstepping	0.0015	0.0124
SMC	0.0010	0.0011
ISMC	0.0013	0.0005
BISMC	0.0009	0.0003
DISMC with GPR	0.0008	0.0003

Control commands shown in Figure 9 verify that the proposed method provides less chattering compared to the ISMC and SMC. Consequently, numerical simulation results demonstrate that the proposed method converges faster while provided smaller tracking error than the state-of-art approaches.

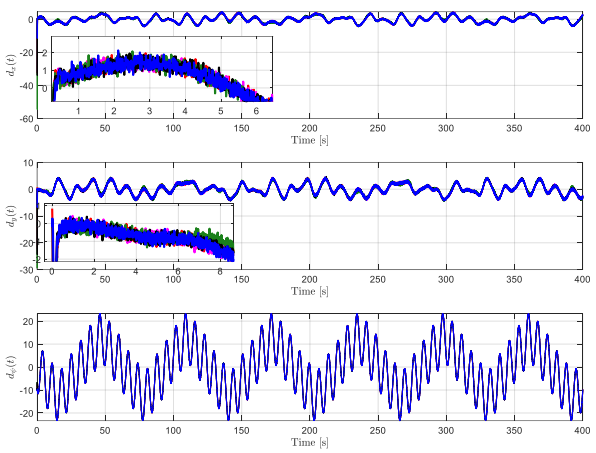

Fig. 10 Case I: Displays the lumped disturbances in all three degrees of freedom under the BS, SMC, ISMC, BISMC, and DISMC with GPR

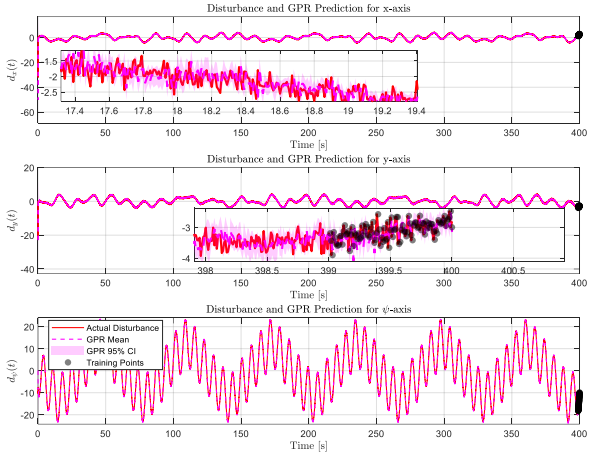

Fig. 11 Case I: Demonstrates the Gaussian Process Regression (GPR)-based modeling of lumped disturbances under the DISMC with GPR controller

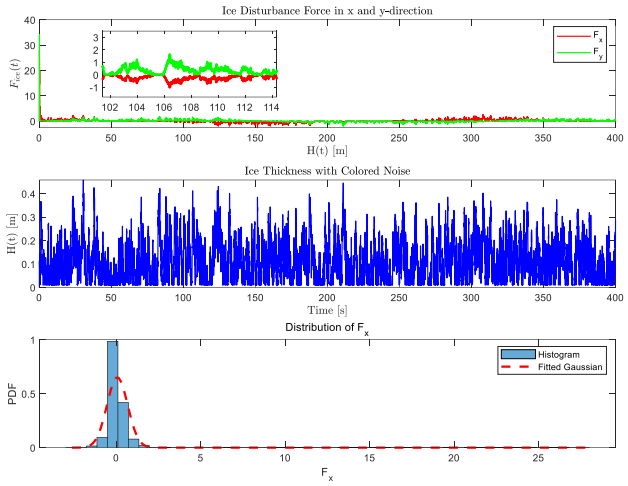

Fig. 12 Case I: Illustrates the forces acting on the USV in the presence of floating ice fragments in the x and y directions, as well as the ice thickness distribution and its probability density function

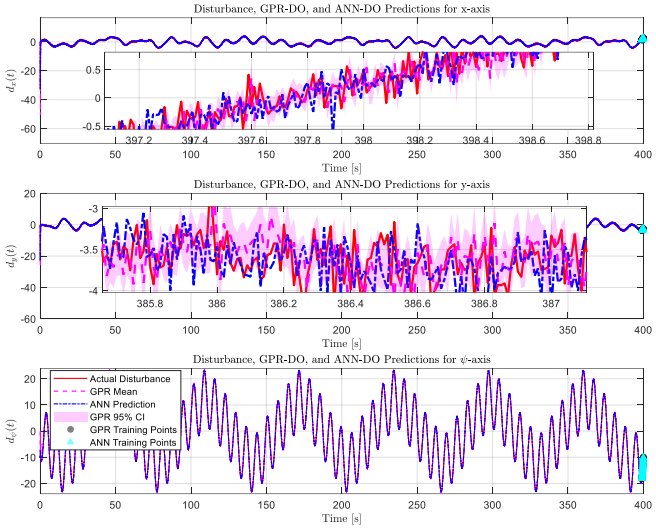

Fig. 13 Case I: Comparison of lumped disturbance predictions using GPR-DO and ANN-DO under ice floe sea states

Figure 10 illustrates the variations of the lumped disturbances acting on the system in the x, y and ψ directions. These disturbances include model uncertainties and external environmental forces.

Figure 11 focuses on the proposed DISMC with Gaussian Process Regression (GPR), showing how GPR models the lumped disturbances. In this method, GPR is employed to estimate the unknown disturbances online and incorporate them into the control law for compensation, thereby enhancing control performance. The figure shows the fitting and prediction results of the GPR model, which closely match the actual disturbances. The accuracy of the GPR-based estimation confirms the effectiveness of the proposed control strategy in handling uncertain and time-varying disturbances.

Figure 12 depicts the forces acting on the system in the x and y directions under a floating ice environment, as well as the ice thickness distribution and its probability density. It is clearly observed that the forces in both directions increase significantly with the thickness of the ice, highlighting the impact of environmental variability on the USV's dynamics.

To validate the efficacy of the proposed GPR-based disturbance observer (GPR-DO) against conventional ANN-based DOs, Fig. 13 illustrates the real-time predictions of lumped disturbances (including stochastic ice floe resistance) across the three degrees of freedom (DOF) for the USV. The actual disturbances,

synthesized via an Ornstein-Uhlenbeck process mimicking ice impacts [4-6], exhibit significant stochastic variations, particularly in the yaw DOF due to rotational torques from floe collisions. As shown, the GPR mean predictions closely track the true disturbances with minimal bias, while the 95% confidence intervals (shaded regions) effectively capture the epistemic uncertainty without prior distributional assumptions - a key advantage over ANN, which relies on deterministic point estimates and shows larger deviations during transient phases (e.g., initial 10-20 s with limited data).

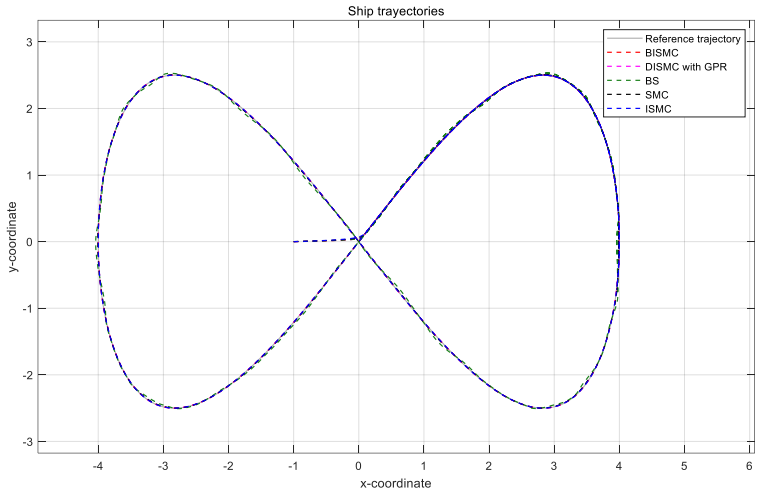

Fig. 14 Case II: Reference trajectory and real trajectory of the USV under the BS, SMC, ISMC, BISMC, and DISMC with GPR

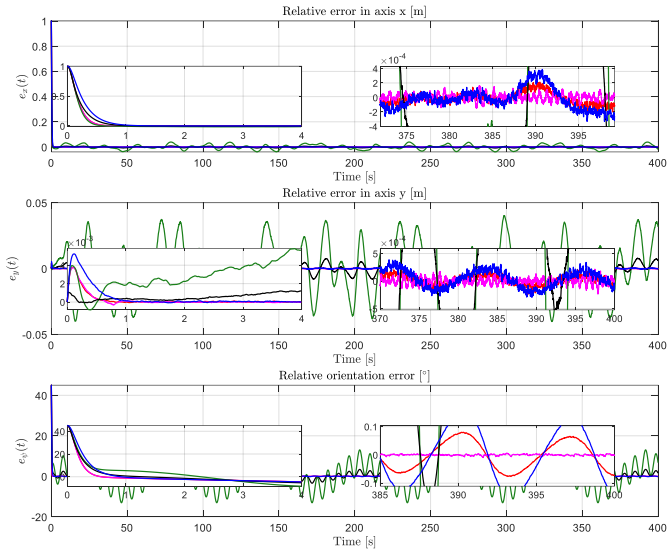

Fig. 15 Case II: Comparison in tracking error in x-axis, y-axis, and ψ-axis under the BS, SMC, ISMC, BISMC, and DISMC with GPR. Tracking errors for with a detailed view for $t \in [370, 400]$

The trajectory tracking results for Case II are shown in Figure 14 and Figure 15. Similar to the previous simulation, the proposed DISMC with GPR generates relatively smooth control inputs, under which the USV converges more rapidly to the desired trajectory. These results further validate the superior tracking performance and robustness of the proposed control scheme, particularly in the presence of environmental disturbances and model uncertainties.

7. Conclusion

In this work, we proposed a discrete integral sliding-mode trajectory tracking control with a disturbance observer based on Gaussian process regression for uncertain unmanned surface vessels operating in ice-

covered ocean areas. The method has ensured precise trajectory tracking under disturbances from winds, waves, currents, and ice floes. We established the stability criterion of the discrete closed-loop system under bounded lumped uncertainties using discrete stochastic system theory and further analyzed stability when the estimation error was Gaussian distributed. Simulation results have demonstrated the superior performance of the proposed method. This study has provided a basis for developing probabilistic observer–based hybrid control approaches, and future work will address input saturation and actuator faults.

ACKNOWLEDGMENTS

This work was supported by the Key R&D projects of China (grant numbers 2021YFC2803400 and 2021YFC2803401).

REFERENCES

[1] Kubat, I., Fowler, C.D., Sayed, M., 2021. Floating Ice and Ice-Pressure Challenge to Ships. In Snow and Ice-Related Hazards, Risks, and Disasters, *Elsevier*, 641–669. https://doi.org/10.1016/B978-0-12-817129-5.00006-8

[2] Knauss, J.A., Garfield, N., 2017. Introduction to Physical Oceanography, third edition ed.; *Waveland Press, Inc*, Long Grove, Illinois, USA.

[3] Li, G., Zhang, X., 2022. Research on the influence of wind, waves, and tidal current on ship turning ability based on Norrbin model. *Ocean Engineering*, 259, 111875. https://doi.org/10.1016/j.oceaneng.2022.111875

[4] Huang, L., Tuhkuri, J., Igrec, B., Li, M., Stagonas, D., Toffoli, A., Cardiff, P., Thomas, G., 2020. Ship resistance when operating in floating ice floes: A combined CFD&DEM approach. *Marine Structures*, 74, 102817. https://doi.org/10.1016/j.marstruc.2020.102817

[5] Huang, L., Li, Z., Ryan, C., Ringsberg, J.W., Pena, B., Li, M., Ding, L., Thomas, G., 2021. Ship resistance when operating in floating ice floes: Derivation, validation, and application of an empirical equation. *Marine Structures*, 79, 103057. https://doi.org/10.1016/j.marstruc.2021.103057

[6] Zhao, W., Leira, B.J., Feng, G., Gao, C., Cui, T., 2021. A reliability approach to fatigue crack propagation analysis of ship structures in polar regions. *Marine Structures*, 80, 103075. https://doi.org/10.1016/j.marstruc.2021.103075

[7] Fang, M.C., Lin, Y.H., Wang, B.J., 2012. Applying the PD controller on the roll reduction and track keeping for the ship advancing in waves. *Ocean Engineering*, 54, 13–25. https://doi.org/10.1016/j.oceaneng.2012.07.006

[8] Fang, M.C., Zhuo, Y.Z., Lee, Z.Y., 2010. The application of the self-tuning neural network PID controller on the ship roll reduction in random waves. *Ocean Engineering*, 37, 529–538. https://doi.org/10.1016/j.oceaneng.2010.02.013

[9] Guan, W., Xi, Z., Cui, Z., Zhang, X., 2025. Adaptive trajectory controller design for unmanned surface vehicles based on SAC-PID. *Brodogradnja*, 76(2), 1-22. https://doi.org/10.21278/brod76206

[10] He, W., Yin, Z., Sun, C., 2017. Adaptive neural network control of a marine vessel with constraints using the asymmetric barrier Lyapunov function. *IEEE Transactions on Cybernetics*, 47, 1641–1651. https://doi.org/10.1109/TCYB.2016.2554621

[11] Larrazabal, J.M., Peñas, M.S., 2016. Intelligent rudder control of an unmanned surface vessel. *Expert Systems with Applications*, 55, 106–117. https://doi.org/10.1016/j.eswa.2016.01.057

[12] Ashrafiuon, H., Muske, K., McNinch, L., Soltan, R., 2008. Sliding-mode tracking control of surface vessels. *IEEE Transactions on Industrial Electronics*, 55, 4004–4012. https://doi.org/10.1109/TIE.2008.2005933

[13] Wen, G., Ge, S.S., Chen, C.L.P., Tu, F., Wang, S., 2019. Adaptive tracking control of surface vessel using optimized backstepping technique. *IEEE Transactions on Cybernetics*, 49, 3420–3431. https://doi.org/10.1109/TCYB.2018.2844177

[14] Witkowska, A., ´Smierzchalski, R., 2018. Adaptive backstepping tracking control for an over-actuated DP marine vessel with inertia uncertainties. *International Journal of Applied Mathematics and Computer Science*, 28, 679–693. https://doi.org/10.2478/amcs-2018-0052

[15] Liu, Z., 2019. Practical backstepping control for underactuated ship path following associated with disturbances. *IET Intelligent Transport Systems*, 13, 834–840. https://doi.org/10.1049/iet-its.2018.5448

[16] Zheng, H., Wu, J., Wu, W., Zhang, Y., 2020. Robust dynamic positioning of autonomous surface vessels with tube-based model predictive control. *Ocean Engineering*, 199, 106820. https://doi.org/10.1016/j.oceaneng.2019.106820

[17] Zhang, J., Sun, T., Liu, Z., 2017. Robust model predictive control for path-following of underactuated surface vessels with roll constraints. *Ocean Engineering*, 143, 125–132. https://doi.org/10.1016/j.oceaneng.2017.07.057

[18] Yan, Z., Wang, J., 2012. Model predictive control for tracking of underactuated vessels based on recurrent neural networks. *IEEE Journal of Oceanic Engineering*, 37, 717–726. https://doi.org/10.1109/JOE.2012.2201797

[19] Zhang, Y., Zhang, J., Guo, Z., Zhang, L., Shang, Y., 2025. An adaptive NMPC for ROVs trajectory tracking with environmental disturbances and model uncertainties. *Brodogradnja*, 76(1), 1-25. https://doi.org/10.21278/brod76106

[20] Lu, X., Liu, Z., Chu, Z., 2020. Nonlinear adaptive heading control for an underactuated surface vessel with constrained input and sideslip angle compensation. *Brodogradnja*, 71(3), 71-87. https://doi.org/10.21278/brod71305

[21] Yan, He, Y., Zhao, X., Huang, L., Xu, L., Liu, J., 2024. Control method for the ship track and speed in curved channels. *Brodogradnja*, 75(3), 1-27. https://doi.org/10.21278/brod75307

[22] Zhang, J., Liu, X., Xia, Y., Zuo, Z., Wang, Y., 2016. Disturbance observer-based integral sliding-mode control for systems with mismatched disturbances. *IEEE Transactions on Industrial Electronics*, 63, 7040–7048. https://doi.org/10.1109/TIE.2016.2583999

[23] Liu, J., Gai, W., Zhang, J., Li, Y., 2019. Nonlinear adaptive backstepping with ESO for the quadrotor trajectory tracking control in the multiple disturbances. *International Journal of Control*, Automation and Systems, 17, 2754–2768. https://doi.org/10.1007/s12555-018-0909-9

[24] Yin, S., Xiao, B., 2017. Tracking control of surface ships with disturbance and uncertainties rejection capability. *IEEE/ASME Transactions on Mechatronics*, 22, 1154–1162. https://doi.org/10.1109/TMECH.2016.2618901

[25] Van, M., 2019. Adaptive neural integral sliding-mode control for tracking control of fully actuated uncertain surface vessels. *International Journal of Robust and Nonlinear Control*, 29, 1537–1557. https://doi.org/10.1002/rnc.4455

[26] Van, M., 2019. An enhanced tracking control of marine surface vessels based on adaptive integral sliding mode control and disturbance observer. *ISA Transactions*, 90, 30–40. https://doi.org/10.1016/j.isatra.2018.12.047

[27] Elbrachter, D., Perekrestenko, D., Grohs, P., Bolcskei, H., 2021. Deep neural network approximation theory. *IEEE Transactions on Information Theory*, 67, 2581–2623. https://doi.org/10.1109/TIT.2021.3062161

[28] Barrau, A., Bonnabel, S., 2017. The invariant extended Kalman filter as a stable observer. *IEEE Transactions on Automatic Control*, 62, 1797–1812. https://doi.org/10.1109/TAC.2016.2594085

[29] Bishop, C.M., 2006. Pattern recognition and machine learning (information science and statistics), *Springer New York*.

[30] Murphy, K.P., 2012. Machine Learning: A Probabilistic Perspective; Adaptive Computation and Machine Learning Series, *MIT Press*, Cambridge, MA.

[31] Osinenko, P., Yaremenko, G., Malaniya, G., 2023. On Stochastic Stabilization via Nonsmooth Control Lyapunov Functions. *IEEE Transactions on Automatic Control*, 68, 4925–4931. https://doi.org/10.1109/TAC.2022.3211986

[32] Tatari, F., Modares, H., 2023. Deterministic and stochastic fixed-time stability of discrete-time autonomous systems. *IEEE/CAA Journal of Automatica Sinica*, 10, 945–956. https://doi.org/10.1109/JAS.2023.123405

[33] Jiang, C., Wu, C., Xiao, X., Lin, C., 2023. Robust neural dynamics with adaptive coefficient applied to solve the dynamic matrix square root. *Complex & Intelligent Systems*, 9, 4213–4226. https://doi.org/10.1007/s40747-022-00954-9

[34] Du, J., Hu, X., Krstić, M., Sun, Y., 2016. Robust dynamic positioning of ships with disturbances under input saturation. *Automatica*, 73, 207–214. https://doi.org/10.1016/j.automatica.2016.06.020

[35] Qin, J., Ma, Q., Gao, H., Zheng, W.X., 2018. Fault-tolerant cooperative tracking control via integral sliding mode control technique. *IEEE/ASME Transactions on Mechatronics*, 23, 342–351. https://doi.org/10.1109/TMECH.2017.2775447

[36] Fossen, T.I., 2011. Handbook of Marine Craft Hydrodynamics and Motion Control, 1 ed.; *Wiley*,. https://doi.org/10.1002/9781119994138

[37] Qin, Y., Cao, M., Anderson, B.D.O., 2020. Lyapunov criterion for stochastic systems and its applications in distributed computation. *IEEE Transactions on Automatic Control*, 65, 546–560. https://doi.org/10.1109/TAC.2019.2910948

[38] Zong, Z., Zhou, L., 2019. A theoretical investigation of ship ice resistance in waters covered with ice floes. *Ocean Engineering*, 186, 106114. https://doi.org/10.1016/j.oceaneng.2019.106114

[39] Xue, Y., Zhong, K., Ni, B.Y., Li, Z., Bergström, M., Ringsberg, J.W., Huang, L., 2024. A combined experimental and numerical approach to predict ship resistance and power demand in broken ice. *Ocean Engineering*, 292, 116476. https://doi.org/10.1016/j.oceaneng.2023.116476